Letters in Applied NanoBioScience
Open-Access Journal (ISSN: 2284-6808)

Article
Volume 12, Issue 1, 2023, 14
https://doi.org/10.33263/LIANBS121.014

Exploring the Crystal, FT-IR, Optical, and NLO Properties of 3,4-Dichloro-6-Ehtyl-6H-Pyrano[3,2-c]Quinoline-2,5-Dione (DCPQ)

Athisaya Rajah Suvitha [1], Mohamed Ahmed Mohamed El-Mansy [2,3*]

[1] Department of Physics, CMR Institute of Technology, Bengaluru, Karnataka, India
[2] Molecular Modeling Simulation Lab., Department of Physics, Faculty of Education, Ain Shams University, Roxy, Cairo, Egypt
[3] Condensed Matter Theory Group, Department of Physics, College of Science and Arts, Qassim University, Ar Rass, 51921, Saudi Arabia
* Correspondence: Profmelmansy@gmail.com (M.A.M.E.M.);

Scopus Author ID 35751222700
Received: 10.24.2021; Accepted: 5.12.2021; Published: 9.01.2022

Abstract: Theoretical calculations are fulfilled via DFT_B3PW91_SDD for DCPQ molecule. The experimental IR spectrum is scanned in the range 500–4000 cm^{-1} and compared with calculated IR. Detailed IR assignments are aided using GV5.0.9 program. The accuracy of calculation level is acknowledged by established agreement among recorded and computed wavenumbers. Frontier analysis for DCPQ molecular orbitals shows a considerable bandgap offset (3.78 eV) and overall dipole moment (TDM=7.64 D). Such results push DCPQ forward to be a highly active and more efficient replacer for current Si & Ge photovoltaics. Also, DCPQ reveal a remarkable NLO response ($\beta_{DCPQ} = 4.29 * 10^{-30}$esu $\sim 12\beta_{urea}$ that made DCPQ a prime candidate for forthcoming NLO devices.

Keywords: DCPQ; DFT_B3PW91_SDD; FT-IR; TDM; HOMO/LUMO offset; Polarizability; 1st hyperpolarizability.

© 2022 by the authors. This article is an open-access article distributed under the terms and conditions of the Creative Commons Attribution (CC BY) license (https://creativecommons.org/licenses/by/4.0/).

1. Introduction

Researchers recently exhibited more effort to prepare and synthesize more heterocyclics, including those present in different bioactive alkaloids [1-4]. Pyranoquinoline derivatives became favorable structures in nonlinear optical (NLO) fabricated devices [5-8] and in medicine due to their hygienic [9] and bacteriolytic activities [10]. Also, as AChE [11], allergy [12], and inflame restraints [13]. They act as pharmacophores versus psychotropics, sexual-transmitted diseases [14], and anticancer treatment [15]. Styryl-quinolines and Au(III) base-dithiolene complexes are considered efficient materials for NLO applications [6,16]. Also, many quinoline derivatives are used as corrosion inhibitors for iron [17], and pyrano-pyrimidines tagged with coumarin substituents are utilized as DNA gyrase inhibitors [18]. Organic photovoltaics are characterized by fair cost fabrication and high competencies for energy conversion [19,20]. The active challenge is exploring a considerable photo-current by synthesizing novel organic photovoltaic devices [21,22]. Pyrano-quinoline-2-one derivatives are distinguished by their antitumor/antioxidant activities, proteins monitoring, and anti-fungal/-bacterial medication synthesis [23]. Authors prepare 3,4-dichloro-6-ehtyl-6H-pyrano[3,2-c]quinoline-2,5-dione (DCPQ) framework ($C_{14}H_9Cl_2NO_3$) to be the interest of the

current research. The current research is the first trial to report structural, electronic, FT-IR, optical, and nonlinear optical (NLO) properties for DCPQ molecules. Density-Functional-Theorem (DFT) considering Becke3/Perdew/Wang (B3PW91) level is applied to explore crystal [24,25], IR, frontier features [20,22,26-30]. DCPQ thermochemistry, HOMO-LUMO offset, total dipole-moment (TDM), and nonlinear optical (NLO) calculations are accomplished at the same method. The current research issue is to explore expected physical characteristics for DCPQ and its proper applications in photovoltaic and NLO technologies.

2. Materials and Methods

2.1. FT-IR measurements.

A well-prepared DCPQ/KBr desk (50:1) is used to detect FT-IR spectrum in the range 500–4000 cm^{-1} at chamber temperature via BRUKER_IFS_66V device.

2.2. Computational details.

Theoretical computations are completed using DFT/ B3PW91_SDD level through both G09W and GV5.0.9 soft/codes [31-42]. First, optimized DCPQ structure is calculated, and assorted crystal parameters (bond length (Å) & bond angle (°)) are registered in Table 1. Figure 1 shows the optimum DCPQ geometry. Second, the optimized structure output is applied for IR frequency calculations at the same level. The experimental, theoretical wavenumbers and corresponding assignments are presented in Table 2. A comparative observed and calculated IR chart-indexing are highlighted in Figure 2. After that, Mulliken distributions are performed to show electron carry through the whole DCPQ molecule. Detailed information concerning donor/acceptor atom nature is maintained in Table 3. In addition, Thermochemistry aspects, total dipole moment (TDM), HOMO/LUMO offset, ionizing potential (I), electronic affinity (A), hardness (η), electronic potential (μ), electrophilic index (Ψ) and lastly softness (ζ) are computed and registered in Table 4. Finally, DCPQ nonlinear optical (NLO) features such as polarizability (α) and 1st order hyperpolarizability (β) are fulfilled in Table 5.

3. Results and Discussion

3.1. Crystal and FT-IR analyses.

DCPQ crystal parameters (bond lengths & bond angles) at B3PW91_SDD are imported into Table 1. The optimal bond length for C=C is in the range 1.38∼1.43 Å that compares well with the experimental value 1.48 Å. The C=O bond length in the range 1.25 to 1.43 Å is much extended than the experimental index 1.23 Å [43]. The C-N bond length in the range 1.40∼1.48 Å is wild stretched than experiment 1.27 ∼1.35 Å [44]. Such agreement between computed and experimental data acknowledged our selected calculation level as a precise crystallographic technique.

In a nonlinear framework, the vibrational modes are counted via formula 3N-6, where N is the atoms-sum. So, DCPQ framework ($C_{14}H_9Cl_2NO_3$) as 81 (64 actives & 17 inactive) modes. Only 17 modes are picked up to concord with recorded wavenumbers assigned in Table 2. The imposed assignments are based upon GV5.0.9 outputs for experimental/theoretical IR mapped indices. Figure 3 shows both DCPQ observed and calculated IR charts. The extended H-antennas and bulk interactions may interfere with agreement among measurable (solid-

phase) and calculated (gas-phase) results to some extent. In brief, DCPQ assignments are summarized as:

N-H stretch is detected via 3300~3500 cm^{-1} [45-47]. Mode (1) is registered as N-H stretch at 3300 cm^{-1}, comparable to the measured value at 3347 cm^{-1}. Modes (10,14) are assigned to N-H in/out of the plane bend at 1340 cm^{-1} and 850 cm^{-1}, corresponding to observed peaks at 1285 cm^{-1} and 830 cm^{-1}, respectively. C-H stretch (aromatic/aliphatic) is perceived among 3200~2900 cm^{-1} [48-50]. Modes (2, 4) are specified to aromatic and asymmetric/symmetric C-H stretch at 3200, 3100, 2960 cm^{-1}, agreed with observed data at 3130, 2988, 2945 cm^{-1}, respectively. Modes (10-12) are specified as C-H plane/in the bend at 1250, 1200 cm^{-1}, proportionate to experiment at 1250, 1183 cm^{-1}. Mode (15) is related to the C-H plane/out bend at 765 cm−1, matching the identified band at 765 cm^{-1}. C=O stretch is noticed around 1760-1690 cm^{-1} [51-53]. Mode (5) is specified for C=O stretching at 1760 cm^{-1}, concours with the recorded band at 1746 cm^{-1}. Modes (6, 8) are referred to C=C stretch at 1660, 1620, 1580 cm^{-1}, comparable to experimental results at 1670, 1643, 1500 cm^{-1}. Mode (13) is related to C-O + C-N + C-C stretch at 960 cm−1, analogous to measured peak at 950 cm^{-1} [54-56]. Modes (16,17) are specified for C-O + C-N + C-C Plane in/out bend at 666, 586 cm^{-1}, corresponds to measurements at 698, 580 cm^{-1}, respectively. Finally, Mode (9) is assigned as CH_3 deformation at 1450 cm^{-1}, agreed with a scanned peak at 1466 cm^{-1}.

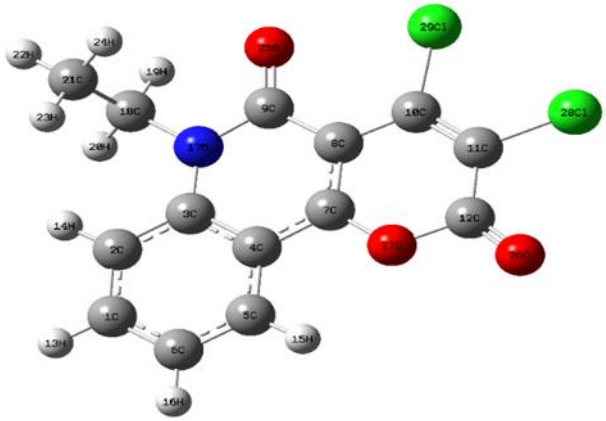

Figure 1. The optimized DCPQ model.

Table 1. Crystal parameters for DCPQ.

Bond Length (Å)	B3PW91_SDD	Bond Angle (°)	B3PW91_SDD	Bond Angle (°)	B3PW91_SDD
C1-C2	1.39	C2-C1-C6	121.20	C12-C11-Cl28	114.57
C1-C6	1.41	C2-C1-H13	119.05	C11-C12-O26	129.00
C1-H13	1.09	C6-C1-H13	119.75	C11-C12-O27	113.44
C2-C3	1.42	C1-C2-C3	120.29	O26-C12-O27	117.57
C2-H14	1.08	C1-C2-H14	118.96	C2-H14-H23	106.80
C3-C4	1.42	C3-C2-H14	120.75	C3-N17-C9	124.07
C3-N17	1.40	C2-C3-C4	118.35	C3-N17-C18	120.62
C4-C5	1.42	C2-C3-N17	122.20	C9-N17-C18	115.29
C4-C7	1.43	C4-C3-N17	119.45	N17-C18-H19	106.42
C5-C6	1.39	C3-C4-C5	120.58	N17-C18-H20	108.36
C5-H15	1.08	C3-C4-C7	117.81	C17-C18-C21	112.62
C6-H16	1.09	C5-C4-C7	121.62	H19-C18-H20	107.93
C7-C8	1.39	C4-C5-C6	120.33	H19-C18-C21	109.34
C7-O27	1.37	C4-C5-H15	118.43	H20-C18-C21	111.93
C8-C9	1.48	C6-C5-H15	121.24	C18-C21-H22	109.76
C8-C10	1.45	C1-C6-C5	119.25	C18-C21-H23	112.14
C9-N17	1.42	C1-C6-H16	120.31	C18-C21-H24	110.13
C9-O25	1.25	C5-C6-H16	120.44	H22-C21-H23	108.22
C10-C11	1.38	C4-C7-C8	123.30	H22-C21-H24	107.98
C10-Cl29	1.78	C4-C7-O27	114.79	H23-C21-H24	108.51
C11-C12	1.46	C8-C7-O27	121.91	H14-H23-C21	104.34

Bond Length (Å)	B3PW91_SDD	Bond Angle (°)	B3PW91_SDD	Bond Angle (°)	B3PW91_SDD
C11-Cl28	1.78	C7-C8-C9	118.82	C7-O27-C12	124.14
C12-O26	1.23	C7-C8-C10	116.95		
C12-O27	1.43	C9-C8-C10	124.23		
H14-H23	2.48	C8-C9-N17	116.46		
N17-C18	1.48	C8-C9-O25	124.21		
C18-H19	1.09	N17-C9-O25	119.33		
C18-H20	1.09	C8-C10-C11	120.93		
C18-C21	1.53	C8-C10-Cl29	121.10		
C21-H22	1.10	C11-C10-Cl29	117.97		
C21-H23	1.10	C10-C11-C12	122.62		
C21-H24	1.09	C10-C11-Cl28	122.81		

Table 2. DCPQ IR wavenumbers indexing and corresponding assignments.

No	Exp. (cm^{-1})	B3PW91_SDD Cal. (cm^{-1})	Assignments
1	3347	3300	υ N-H
2	3130	3200	υ C-H (aromatic)
3	2988	3100	$υ_{as}$ C-H (aliphatic)
4	2945	2960	$υ_s$ C-H (aliphatic)
5	1746	1760	υ C=O
6	1670	1660	υ C=C
7	1643	1620	
8	1500	1580	
9	1466	1450	CH_3 Deformation
10	1285	1340	β N-H
11	1250	1250	β C-H
12	1183	1200	
13	950	960	υ C-O & υ C-N & υ C-C
14	830	850	γ N-H
15	765	765	γ C-H
16	698	666	β C-O & β C-N & β C-C
17	580	586	γ C-O & γ C-N & γ C-C

υ; setrching, $υ_{as}$; asymmetric stretching, $υ_s$; symmetric stretching; β; inplane bending, γ; outplane bending

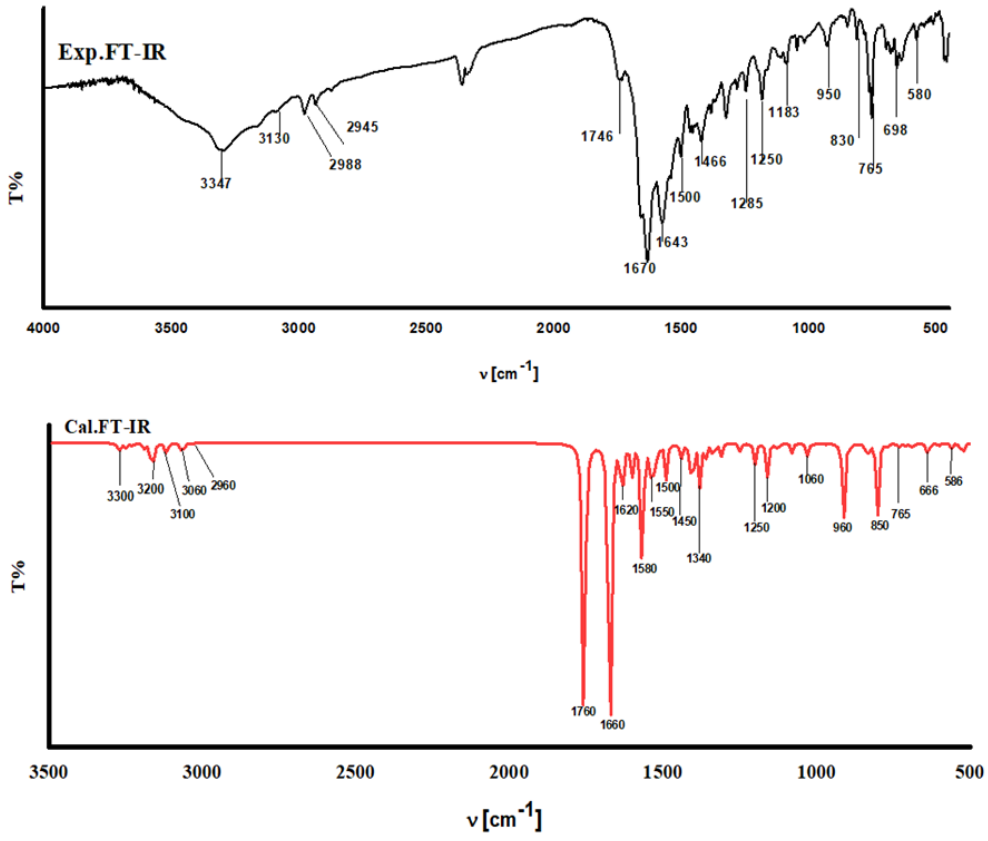

Figure 2. The Observed & Computed DCPQ IR-Charts.

3.2. Mulliken distributions.

Mulliken distributions are vital tools that point out electron rush, electronegativity, and molecule's electron-arrays [57-59]. Distinctive Mulliken distribution for DCPQ electrons rush are in Table 3 and well-presented in Figure 4. Results showed that O, N, and nearby C atoms have electron excess that provides negative charges around. Such a high electron rush towards high electronegative centers will cause electrons deficiencies at other C atoms and hydrogen antennae that provide positive charges around. Such electron-rush variance in DCPQ will influence photovoltaic and nonlinear optical (NLO) features[60-63].

Table 3. Mulliken distributions for DCPQ at B3PW91_SDD.

Donors	Q (a. u)	Acceptors	Q (a. u)
C(3)	0.2836	C(1)	-0.2363
C(4)	0.1856	C(2)	-0.3207
C(7)	0.2865	C(5)	-0.3278
C(8)	0.1743	C(6)	-0.2557
C(9)	0.1410	C(10)	-0.0521
C(12)	0.2558	C(11)	-0.2965
		C(18)	-0.3463
H(13)	0.2306	C(21)	-0.6474
H(14)	0.2477		
H(15)	0.2798	N(17)	-0.3200
H(16)	0.2375		
H(19)	0.2747	O(25)	-0.2899
H(20)	0.2166	O(26)	-0.2047
H(22)	0.2192	O(27)	-0.3189
H(23)	0.2157		
H(24)	0.2491		
Cl(28)	0.0434		
Cl(29)	0.0752		

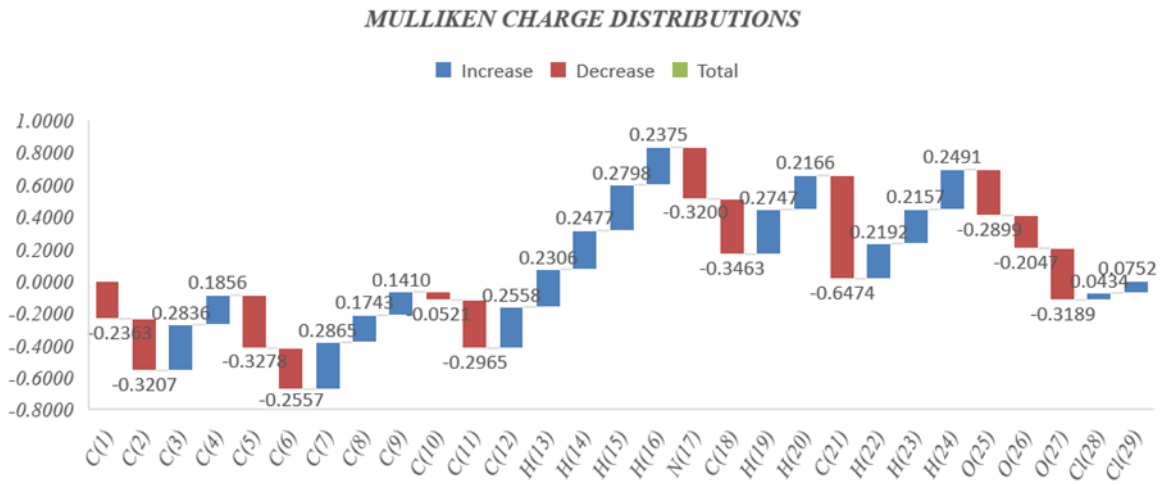

Figure 3. DCPQ Mulliken charge distributions.

3.3. Thermochemistry, FMOs & NLO analyses.

Essential physical indices are deduced via HOMOs and LUMOs energies such as ionization_potential $\boldsymbol{I = -E_{HOMO}}$, electronic_affinity $\boldsymbol{A = -E_{LUMO}}$, hardness $\eta = \frac{1}{2}(\boldsymbol{E_{LUMO} - E_{HOMO}})$, electronic_potential $\boldsymbol{\mu} = \frac{1}{2}(\boldsymbol{E_{LUMO} + E_{HOMO}})$, electrophilic index $\boldsymbol{\psi = \mu^2 / 2}\eta$, and softness $\boldsymbol{\zeta = 1/}\eta$ [64]. Spaciously, other physical parameters are listed (cf., Table 4) as ground & zero energies ($\boldsymbol{G.E}$ & $\boldsymbol{Z.E}$), entropy ($\boldsymbol{S}$), specific heat ($\boldsymbol{C_V}$), total dipole moment, and $E_{LUMO/HOMO}$ for DCPQ at the same level.

Table 4. Thermochemistry of DCPQ at B3PW91_SDD.

Parameter	DCPQ B3PW91_SDD		DCPQ B3PW91_SDD
G. E(Hartree)	-1739.14521623	Z.E(Kcal/Mol)	129.243
TDM(Debye)	7.64	S (Cal/Mol-°K)	
Spin	Singlet	Total	132.338
E_{LUMO}(eV)	-3.02	Translational	43.081
E_{HOMO}(eV)	-6.79	Vibrational	54.930
$E_{LUMO/HOMO}$(eV)	3.78	Rotational	34.327
I (eV)	3.02	Total	
A (eV)	6.79	C_V (Cal/Mol-°K)	
η (eV)	1.88	Total	63.146
μ (eV)	-4.90	translational	2.981
ψ (eV)	6.38	Vibrational	57.184
ζ (eV^{-1})	0.53	Rotational	2.981

$E_{LUMO/HOMO}$ is a precise measure for electron rush amongst molecular states [65,66]. Figure 4 represents DCPQ energy gap. DCPQ holds over TDM (7.64 D) and HOMO/LUMO offset (3.78 eV). As well-known, the doorstep electron/hole pair generation for Si & Ge solar cells are 3.9 eV and 2.8 eV, respectively [67,68]. Accordingly, DCPQ may be the next competitor candidate for upcoming photovoltaic devices.

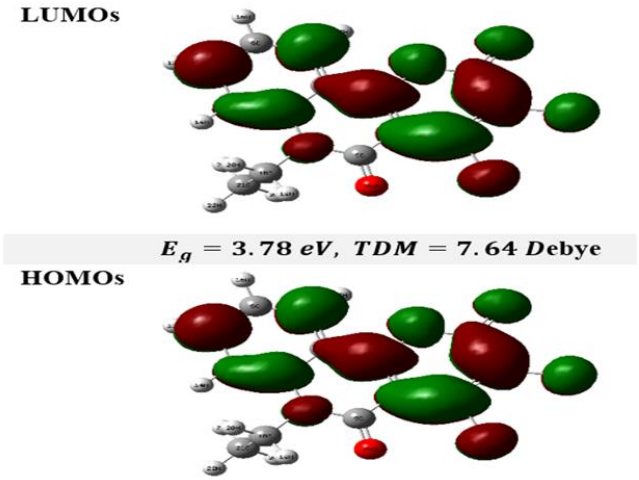

Figure 4. Bandgap offset for DCPQ molecule.

Utilizing G09W logfiles, authors extract both DCPQ polarizability (α_{xx}; α_{xy}; α_{yy}; α_{xz}; α_{yz}& α_{zz}) and 1st hyperpolarizability (β_{xxx}; β_{xxy}; β_{xyy}; β_{yyy}; β_{xxz}; β_{xyz}; β_{yyz}; β_{xzz}; β_{yzz} & β_{zzz}) indices. The total polarizability (α_{tot}), polarizability anisotropy ($\Delta\alpha$) and 1st hyperpolarizability (β_{tot}) are computed via the assorted empirical forms [69]:

$$\boldsymbol{\alpha_{tot} = \frac{\alpha_{xx} + \alpha_{yy} + \alpha_{zz}}{3}}$$

$$\boldsymbol{\Delta\alpha = \frac{1}{\sqrt{2}}\left[(\alpha_{xx} - \alpha_{yy})^2 + (\alpha_{yy} - \alpha_{zz})^2 + (\alpha_{zz} - \alpha_{xx})^2 + 6\alpha_{yz}^2 + 6\alpha_{xy}^2 + 6\alpha_{xz}^2\right]^{1/2}}$$

$$\boldsymbol{\beta_{tot} = \left[(\beta_{xxx} + \beta_{xyy} + \beta_{xzz})^2 + (\beta_{yyy} + \beta_{yzz} + \beta_{yxx})^2 + (\beta_{zzz} + \beta_{zxx} + \beta_{zyy})^2\right]^{1/2}}$$

The $\boldsymbol{\alpha_{tot}}$, $\boldsymbol{\Delta\alpha}$ *and* $\boldsymbol{\beta_{tot}}$ for DCPQ are registered in Table 5. The computed 1st hyperpolarizability (β_{tot}) for DCPQ is 4.29 * 10^{-30} esu that is 12 times overestimated than for urea (ref. β_{urea} = 0.3728 x10^{-30} esu). Such hyperpolarizability nominates DCPQ as potential material for forthcoming NLO devices.

Table 5. Mean polarizability $\boldsymbol{\alpha_{tot}}$, polarizability anisotropy $\Delta\boldsymbol{\alpha}$ & 1st hyperpolarizability $\boldsymbol{\beta_{tot}}$ for DCPQ.

	B3PW91_SDD $\boldsymbol{\alpha(*10^{-24}esu)}$		**B3PW91_SDD** $\boldsymbol{\beta(*10^{-30}esu)}$
α_{xx}	42.37	β_{xxx}	1.47
α_{xy}	-1.60	β_{xxy}	1.63
α_{yy}	33.48	β_{xyy}	2.50
α_{xz}	-0.51	β_{yyy}	-3.05
α_{yz}	-0.66	β_{xxz}	-0.23
α_{zz}	11.65	β_{xyz}	-0.20
α_{tot}	29.17	β_{yyz}	0.06
$\Delta\alpha$	27.55	β_{xzz}	-0.12
		β_{yzz}	0.07
		β_{zzz}	-0.01
		β_{tot}	4.29

4. Conclusions

A detailed study for structural, IR, optical, and NLO properties is fulfilled utilizing B3PW91_SDD level. Both recorded and computed IR charts indexing approved the precise of the nominated calculation level. Thermochemistry and FMOs analysis are calculated at the same level, which showed that DCPQ possesses TDM (7.64 D) and HOMO/LUMO offset (3.78 eV). Also, 1st hyperpolarizability (β_{tot}) for DCPQ is 4.29 * 10^{-30} esu that is 12 times overestimated that for urea. Such remarkable results upgrade DCPQ as a prime competitor for upcoming photovoltaics and NLO fabricated devices.

Funding

This research received no external funding.

Acknowledgments

This research has no acknowledgment.

Conflicts of Interest

The authors declare no conflict of interest.

References

1. Alizadeh, A.; Rostampoor, A. An efficient synthesis of novel functionalized benzo [h] pyrano [2, 3-b] quinolines and pyrano [2, 3-b] quinoline derivatives via one-pot multicomponent reactions. *Journal of the Iranian Chemical Society* **2021**, 1-11, https://doi.org/10.1007/s13738-021-02376-9.
2. Kaminwar, N.S.; Tekale, S.U.; Pokalwar, R.U.; Kótai, L.; Pawar, R.P. An Efficient and Rapid Synthesis of 1, 4-Dihydropyrano [2, 3-c] Pyran and 1, 4-Dihydropyrano [2, 3-c] Quinoline Derivatives Using Copper Nanoparticles Grafted on Carbon Microspheres. *Polycyclic Aromatic Compounds* **2021**, 1-9, https://doi.org/10.1080/10406638.2021.1950194.
3. Ghiuță, I.; Cristea, D. 15 - Silver nanoparticles for delivery purposes. In: *Nanoengineered Biomaterials for Advanced Drug Delivery*. Mozafari, M. Ed.; Elsevier: **2020;** pp. 347-371, https://doi.org/10.1016/B978-0-08-102985-5.00015-2.
4. Lv, X.; Tang, Y.; Tian, Q.; Wang, Y.; Ding, T. Ultra-stretchable membrane with high electrical and thermal conductivity via electrospinning and in-situ nanosilver deposition. *Composites Science and Technology* **2020**, *200*, https://doi.org/10.1016/j.compscitech.2020.108414.
5. Wu, Y.; Zhang, X.; Negi, A.; He, J.; Hu, G.; Tian, S.; Liu, J. Synergistic Effects of Boron Nitride (BN) Nanosheets and Silver (Ag) Nanoparticles on Thermal Conductivity and Electrical Properties of Epoxy Nanocomposites. *Polymers* **2020**, *12*, https://doi.org/10.3390/polym12020426.
6. El-Nahrawy, A.M.; Abou Hammad, A.B.; Khattab, T.A.; Haroun, A.; Kamel, S. Development of electrically conductive nanocomposites from cellulose nanowhiskers, polypyrrole and silver nanoparticles assisted with Nickel (III) oxide nanoparticles. *Reactive and Functional Polymers* **2020**, *149*, https://doi.org/10.1016/j.reactfunctpolym.2020.104533.

7. Lalegani, Z.; Ebrahimi, S.S.; Hamawandi, B.; La Spada, L.; Toprak, M. Modeling, design, and synthesis of gram-scale monodispersed silver nanoparticles using microwave-assisted polyol process for metamaterial applications. *Optical Materials* **2020**, *108*, https://doi.org/10.1016/j.optmat.2020.110381.
8. Jadhav, C.K.; Nipate, A.S.; Chate, A.V.; Gill, C.H. β-Cyclodextrin: An Efficient Supramolecular Catalyst for the Synthesis of Pyranoquinolines Derivatives under Ultrasonic Irradiation in Water. *Polycyclic Aromatic Compounds* **2021**, 1-16, https://doi.org/10.1080/10406638.2021.1886125.
9. Razavi, F.S.; Hajizadeh-Oghaz, M.; Amiri, O.; Morassaei, M.S.; Salavati-Niasari, M. Barium cobaltite nanoparticles: Sol-gel synthesis and characterization and their electrochemical hydrogen storage properties. *International Journal of Hydrogen Energy* **2021**, *46*, 886-895, https://doi.org/10.1016/j.ijhydene.2020.09.196.
10. Mamun, M.S.A.; Hossain, M.; Naime, J.; Dhar, P. Plasmonic Nanosilver Synthesis Using Sonneratia apetala Fruit Extract and Their Catalytic Activity in Organic Dye Degradation. *Journal of Chemical Health Risks* **2020**, *10*, 287-296, https://doi.org/10.22034/jchr.2020.1904366.1155.
11. Ghosh, K.; Tyagi, S.; Gupta, A. Analytical and Immunopharmacological Studies of Flavonoids: Mangifera Indica and Syzygium Cumini. *Biomedical and Pharmacology Journal* **2020**, *13*, 899-906, https://dx.doi.org/10.13005/bpj/1957.
12. Mirza, B.; Croley, C.R.; Ahmad, M.; Pumarol, J.; Das, N.; Sethi, G.; Bishayee, A. Mango (Mangifera indica L.): a magnificent plant with cancer preventive and anticancer therapeutic potential. *Critical Reviews in Food Science and Nutrition* **2021**, *61*, 2125-2151, https://doi.org/10.1080/10408398.2020.1771678.
13. Tchoumi, L.T.; Nchouwet, M.; Kamani, S.P.; Nana, W.Y.; Djimeli, R.D.; Kamanyi, A.; Ngnokam, S. Antimicrobial and antidiarrhoeal activities of aqueous and methanolic extracts of Mangifera indica Linn stem bark (Anarcadiaceae) in Wistar rats. *Advances in Traditional Medicine* **2021**, *21*, 485–498, https://doi.org/10.1007/s13596-020-00470-6.
14. Faber, K.; StÚckler, H.; Kappe, T. Non-steroidal antiinflammatory agents. 1. Synthesis of 4-hydroxy-2-oxo-1, 2-dihydroquinolin-3-yl alkanoic acids by the wittig reaction of quinisatines. *Journal of heterocyclic chemistry* **1984**, *21*, 1177-1181, https://doi.org/10.1002/jhet.5570210450.
15. Burdeos, G.C.; Blank, R.; Wolffram, S. Influence of quercetin on the global DNA methylation pattern in pigs. *Food Function* **2020**, *11*, 7421-7426, https://doi.org/10.1039/D0FO00896F.
16. Khan, H.; Ullah, H.; Aschner, M.; Cheang, W.S.; Akkol, E. Neuroprotective effects of quercetin in Alzheimer's disease. *Biomolecules* **2020**, *10*, https://doi.org/10.3390/biom10010059.
17. Matada, B.S.; Yernale, N.G.; Basha, J.N. Updates on the versatile quinoline heterocycles as anticancer agents. *Physical Sciences Reviews* **2021**, https://doi.org/10.1515/psr-2021-0040.
18. Salama, S.A.; Kabel, A. Taxifolin ameliorates iron overload-induced hepatocellular injury: Modulating PI3K/AKT and p38 MAPK signaling, inflammatory response, and hepatocellular regeneration. *Chemico-Biological Interactions* **2020**, *330*, https://doi.org/10.1016/j.cbi.2020.109230.
19. Fayed, E.A.; Nosseir, E.S.; Atef, A.; El-Kalyoubi, S.A. In vitro antimicrobial evaluation and in silico studies of coumarin derivatives tagged with pyrano-pyridine and pyrano-pyrimidine moieties as DNA gyrase inhibitors. *Molecular Diversity* **2021**, 1-23, https://doi.org/10.1007/s11030-021-10224-4.
20. Cui, Y.; Zhang, X.; Yin, K.; Qi, X.; Zhang, Y.; Zhang, J.; Li, S.; Lin, H. Dibutyl phthalate-induced oxidative stress, inflammation and apoptosis in grass carp hepatocytes and the therapeutic use of taxifolin. *Science of The Total Environment* **2020**, *764*, https://doi.org/10.1016/j.scitotenv.2020.142880.
21. Vrba, J.; Papoušková, B.; Kosina, P.; Lněničková, K.; Valentová, K.; Ulrichová, J. Identification of Human Sulfotransferases Active towards Silymarin Flavonolignans and Taxifolin. *Metabolites* **2020**, *10*, https://doi.org/10.3390/metabo10080329.
22. Šimunková, M.; Valko, M.; Bučinský, L.; Malček, M. Structure functionality relationship of flavonoids (myricetin, morin, taxifolin and 3′, 4′-dihydroxyflavone). A computational study via the cupric ion probe. *Journal of Molecular Structure* **2020**, *1222*, https://doi.org/10.1016/j.molstruc.2020.128923.
23. Wang, R.; Zhu, X.; Wang, Q.; Li, X.; Wang, E.; Zhao, Q.; Wang, Q.; Cao, H. The antitumor effect of taxifolin on lung cancer via suppressing stemness and epithelial-mesenchymal transition in vitro and oncogenesis in nude mice. *Annals Translational Medicine* **2020**, *8*, https://doi.org/10.21037/atm-20-3329.
24. Dereli, Ö.; Sudha, S.; Sundaraganesan, N. Molecular structure and vibrational spectra of 4-phenylsemicarbazide by density functional method. *Journal of Molecular Structure* **2011**, *994*, 379-386, https://doi.org/10.1016/j.molstruc.2011.03.054.
25. Kalaichelvan, S.; Sundaraganesan, N.; Dereli, O.; Sayin, U. Experimental, theoretical calculations of the vibrational spectra and conformational analysis of 2, 4-di-tert-butylphenol. *Spectrochimica Acta Part A: Molecular and Biomolecular Spectroscopy* **2012**, *85*, 198-209, https://doi.org/10.1016/j.saa.2011.09.061.
26. García-Conesa, M.-T.; Larrosa, M. Polyphenol-Rich Foods for Human Health and Disease. *Nutrients* **2020**, *12*, https://doi.org/10.3390/nu12020400.
27. El-Mansy, M.; Suvitha, A.; Osman, W.; Khaled, K.F. Exploring the electronic and optical absorption properties for homo-and hetero-pyrrole-graphene quantum dots. *Journal of Computational Electronics* **2021**, *20*, 1-16, https://doi.org/10.1007/s10825-021-01773-w.

28. El-Mansy, M.; Ibrahim, M.; Suvitha, A.; Abdelsalam, H.; Osman, W.J.C.; Chemistry, T. Boosted electronic, optical, and NLO responses of homo P-nanoclusters via conducting polymeric substituents. *Computational Theoretical Chemistry* **2021**, *1202*, https://doi.org/10.1016/j.comptc.2021.113343.
29. El-Mansy, M.A.; Osman, O.; Mahmoud, A.A.; Elhaes, H.; Ibrahim, M.A. Computational notes on the molecular modeling analyses of flutamide. *Letters in Applied NanoBioScience* **2020**, *9*, 1099-1102, https://doi.org/10.33263/LIANBS92.10991102.
30. El-Mansy, M.A.; Bayoumy, A.M.; Ezzat, H.; El-Sayed, N.; Elhaes, H.; Osman, O.; Mahmoud, A.A.; Ibrahim, A. Modeling the Effect of Hydration on the Electronic and Vibrational Properties of AZT. *Biointerface Research in Applied Chemistry* **2021**, *11*, 9253-9265, https://doi.org/10.33263/BRIAC112.92539265.
31. El-Mansy, M.A. Quantum chemical studies on structural, vibrational, nonlinear optical properties and chemical reactivity of indigo carmine dye. *Spectrochimica Acta Part A: Molecular and Biomolecular Spectroscopy* **2017**, *183*, 284-290, https://doi.org/10.1016/j.saa.2017.04.047.
32. Soliman, H.; Ibrahim, M.; El-Mansy, M.A.; Atef, S. Structural and optical study of nanostructure of 4-cyanopyranoquinolinedione (CPQ) thin films. *Optical Materials* **2017**, *72*, 122-129, https://doi.org/10.1016/j.optmat.2017.05.052.
33. El-Mansy, M.A.; El-Bana, M.; Fouad, S. On the spectroscopic analyses of 3-Hydroxy-1-Phenyl-Pyridazin-6 (2H) one (HPHP): A comparative experimental and computational study. *Spectrochimica Acta Part A: Molecular and Biomolecular Spectroscopy* **2017**, *176*, 99-105, https://doi.org/10.1016/j.saa.2016.12.040.
34. Gulácsi, M.; El-Mansy, M.A.; Gulácsi, Z. Electron-phonon interactions in conducting polymers. *Philosophical Magazine Letters* **2016**, *96*, 67-75, https://doi.org/10.1080/09500839.2016.1150611.
35. Ibrahim, M.; El-Barbary, A.A.; El-Nahass, M.; Kamel, M.; El-Mansy, M.A.; Asiri, A.M. On the spectroscopic analyses of (E)-3-(dicyclopropyl methylene)-dihydro-4-[1-(2, 5 dimethylfuran-3-yl) ethylidene] furan-2, 5-dione. *Spectrochimica Acta Part A: Molecular Biomolecular Spectroscopy* **2012**, *87*, 202-208, https://doi.org/10.1016/j.saa.2011.11.039.
36. El-Nahass, M.; Kamel, M.; El-Barbary, A.; El-Mansy, M.A.; Ibrahim, M. FT-IR spectroscopic analyses of 3-Methyl-5-Pyrazolone (MP). *Spectrochimica Acta Part A: Molecular Biomolecular Spectroscopy* **2013**, *111*, 37-41, https://doi.org/10.1016/j.saa.2013.03.072.
37. El-Mansy, M.A.; El-Nahass, M.; Khusayfan, N.; El-Menyawy, E. DFT approach for FT-IR spectra and HOMO–LUMO energy gap for N-(p-dimethylaminobenzylidene)-p-nitroaniline (DBN). *Spectrochimica Acta Part A: Molecular Biomolecular Spectroscopy* **2013**, *111*, 217-222, https://doi.org/10.1016/j.saa.2013.04.018.
38. Ibrahim, M.; El-Nahass, M.; Kamel, M.; El-Barbary, A.; Wagner, B.; El-Mansy, M.A. On the spectroscopic analyses of thioindigo dye. *Spectrochimica Acta Part A: Molecular Biomolecular Spectroscopy* **2013**, *113*, 332-336, https://doi.org/10.1016/j.saa.2013.05.014.
39. Soliman, H.; Eid, K.M.; Ali, H.; El-Mansy, M.A.; Atef, S. FT-IR spectroscopic analyses of 2-(2-furanylmethylene) propanedinitrile. *Spectrochimica Acta Part A: Molecular Biomolecular Spectroscopy* **2013**, *105*, 545-549, https://doi.org/10.1016/j.saa.2012.12.051.
40. Soliman, H.; Eid, K.M.; Ali, H.; Atef, S.; El-Mansy, M.A. Vibrational spectroscopic analysis of 2-chloro-5-(2, 5-dimethoxy-benzylidene)-1, 3-diethyl-dihydro-pyrimidine-4, 6 (1H, 5H)-dione. *Spectrochimica Acta Part A: Molecular Biomolecular Spectroscopy* **2012**, *97*, 1079-1084, https://doi.org/10.1016/j.saa.2012.07.104.
41. Ismail, M.; Morsy, G.; Mohamed, H.; El-Mansy, M.A.; Abd-Alrazk, M. FT-IR spectroscopic analyses of 4-hydroxy-1-methyl-3-[2-nitro-2-oxoacetyl-2 (1H) quinolinone (HMNOQ). *Spectrochimica Acta Part A: Molecular Biomolecular Spectroscopy* **2013**, *113*, 191-195, https://doi.org/10.1016/j.saa.2013.04.117.
42. El-Barbary, A.; El-Nahass, M.; Kamel, M.; El-Mansy, M.A. FT-IR, FT-Raman spectra and ab initio HF, DFT vibrational analysis of P-methyl acetanilide. *Journal of Applied Sciences Research* **2009**, *11*, 1977-1987.
43. El-Mansy, M.A.; Yahia, I. Spectroscopic notes of Methyl Red (MR) dye. *Spectrochimica Acta Part A: Molecular Biomolecular Spectroscopy* **2014**, *130*, 59-63, https://doi.org/10.1016/j.saa.2014.03.113.
44. El-Mansy, M.A.; Ismail, M. On the spectroscopic analyses of 3-(4-Hydroxy-1-methyl-2-oxo-1, 2-dihydro-quinolin-3-yl)-2-nitro-3-oxo-propionic acid (HMQNP). *Spectrochimica Acta Part A: Molecular Biomolecular Spectroscopy* **2015**, *135*, 704-709, https://doi.org/10.1016/j.saa.2014.07.033.
45. El-Mansy, M.A.; El-Nahass, M. On the spectroscopic analyses of Perylene-66. *Spectrochimica Acta Part A: Molecular Biomolecular Spectroscopy* **2014**, *130*, 568-573, https://doi.org/10.1016/j.saa.2014.03.118.
46. El-Mansy, M.A.; Mostafa, M.; Ibrahim, M. Synthesis, FT-IR, Bandgap Offset, Polarizability and Hyperpolarizability of 3,4-diamino-6-ehtyl-6H-pyrano[3,2- c]quinoline-2,5-dione (DAPQ) and Cu-2DAPQ as a Promising . *Biointerface Research in Applied Chemistry* **2021**, *11*, 8538-8549, https://doi.org/10.33263/BRIAC111.85388549.
47. El-Mansy, M.A.; Ismail, M. Structural, conformational, optical, and nonlinear optical behavior of ethyl (6-ethyl 5, 6-dihydro 4, 5-dioxo 4 H pyrano [3, 2-c] quinolin-3yl) 2-oxoacetate (EPQOA): comparative theoretical and experimental studies. *Optical and Quantum Electronics* **2021**, *53*, 1-19, https://doi.org/10.1007/s11082-021-02749-7.

48. El-Mansy, M.A.; Suvitha, A.; Narayana, B. Exploring crystal, electronic, optical, and NLO properties of ethyl 4-(3, 4-dimethoxy phenyl)-6-methyl-2-thioxo-1, 2, 3, 4-tetrahydro pyrimidine-5-carboxylate (MTTHPC). *Optical and Quantum Electronics* **2021**, *53*, 1-16, https://doi.org/10.1007/s11082-021-03057-w.
49. Lin, Y.; Rajesh, N.; Raghavan, P.S.; Ramasamy, P.; Huang, Y. Crystal growth of two-component new novel organic NLO crystals. *Materials letters* **2002**, *56*, 1074-1077, https://doi.org/10.1016/S0167-577X(02)00680-8.
50. Iramain, M.A.; Castillo, M.V.; Davies, L.; Manzur, M.E.; Brandán, S.A. Structural and SQMFF study of potent insecticide 4′, 4′-DDT combining the FT-IR and FT-Raman spectra with DFT calculations. *Journal of Molecular Structure* **2020**, *1199*, https://doi.org/10.1016/j.molstruc.2019.126964.
51. Iramain, M.A.; Imbarack, E.; Bongiorno, P.L.; Brandán, S. Characterization of potassium (2-phenylacetyl) trifluoroborate salt by using the UV–Visible, FT-IR and FT-Raman spectra. *Journal of Molecular Structure* **2020**, *1200*, https://doi.org/10.1016/j.molstruc.2019.127057.
52. Selvaraj, S.; Rajkumar, P.; Kesavan, M.; Thirunavukkarasu, K.; Gunasekaran, S.; Devi, N.S.; Kumaresan, S. Spectroscopic and structural investigations on modafinil by FT-IR, FT-Raman, NMR, UV–Vis and DFT methods. *Spectrochimica Acta Part A: Molecular Biomolecular Spectroscopy* **2020**, *224*, https://doi.org/10.1016/j.saa.2019.117449.
53. Iramain, M.A.; Ledesma, A.E.; Imbarack, E.; Bongiorno, P.L.; Brandán, S. Spectroscopic studies on the potassium 1-fluorobenzoyltrifluoroborate salt by using the FT-IR, Raman and UV–Visible spectra and DFT calculations. *Journal of Molecular Structure* **2020**, *1204*, https://doi.org/10.1016/j.molstruc.2019.127534.
54. El-Mansy, M.A.; Ibrahim, M.; Suvitha, A.; Abdelsalam, H.; Osman. W. Atef, Boosted electronic, optical, and NLO responses of homo P-nanoclusters via conducting polymeric substituents. *Computational and Theoretical Chemistry* **2021**, *1202*, https://doi.org/10.1016/j.comptc.2021.113343.
55. Maza, S.; Kijatkin, C.; Bouhidel, Z.; Pillet, S.; Schaniel, D.; Imlau, M.; Guillot, B.; Cherouana, A.; Bendeif, E. Synthesis, structural investigation and NLO properties of three 1, 2, 4-triazole Schiff bases. *Journal of Molecular Structure* **2020**, *1219*, https://doi.org/10.1016/j.molstruc.2020.128492.
56. Yadav, S.B.; Sekar, N. Static-and frequency-dependent NLO properties of dithienothiophene and thienothiophene bridges—A computational investigation. *Journal of Theoretical and Computational Chemistry* **2020**, *19*.
57. Mammadova, F.; Ozsinan, S.; Okutan, M.; Dengiz, C. Synthesis, characterization, and theoretical investigation of optical and nonlinear optical (NLO) properties of triazene-based push–pull chromophores. *Journal of Molecular Structure* **2020**, *1220*, https://doi.org/10.1016/j.molstruc.2020.128726.
58. El-Mansy, M.A.; Suvitha, A.; Osman. W.; Khaled, F. Exploring the electronic and optical absorption properties for homo-and hetero-pyrrole-graphene quantum dots. *Journal of Computational Electronics* **2021,** 29, 2387-2402, https://doi.org/10.1007/s10825-021-01773-w.
59. El-Mansy, M.A.; Osman. W.; Abdelsalam, H. The electronic and optical absorption properties of pristine, homo and hetero Bi-nanoclusters. *Chemical Physics* **2021**, *544*, https://doi.org/10.1016/j.chemphys.2021.111113.
60. Saad, H.A.; Youssef, M.M.; Mosselhi, M. Microwave assisted synthesis of some new fused 1, 2, 4-triazines bearing thiophene moieties with expected pharmacological activity. *Molecules* **2011**, *16*, 4937-4957, https://doi.org/10.3390/molecules16064937.
61. Diab, H.M.; Hassan, W.M.; Abdelhamid, I.A.; Elwahy, A.H. Experimental and theoretical study on the regioselective synthesis and reaction of some bis-and poly (3-mercapto-1, 2, 4-triazin-5 (4H)-one) derivatives. *Journal of Molecular Structure* **2019**, *1197*, 244-261, https://doi.org/10.1016/j.molstruc.2019.07.047.
62. Farag, A.; Halim, S.A.; Roushdy, N.; Badran, A.-S.; Ibrahim, M. Facile synthesis and photodetection characteristics of novel nanostructured triazinyliminomethylpyrano [3, 2-c] quinoline-based hybrid heterojunction. *Journal of Molecular Structure* **2020**, *1221*, https://doi.org/10.1016/j.molstruc.2020.128868.
63. Fatma, S.; Bishnoi, A.; Verma, A. Synthesis, spectral analysis (FT-IR, 1H NMR, 13C NMR and UV–visible) and quantum chemical studies on molecular geometry, NBO, NLO, chemical reactivity and thermodynamic properties of novel 2-amino-4-(4-(dimethylamino) phenyl)-5-oxo-6-phenyl-5, 6-dihydro-4H-pyrano [3, 2-c] quinoline-3-carbonitrile. *Journal of Molecular Structure* **2015**, *1095*, 112-124, https://doi.org/10.1016/j.molstruc.2015.04.026.
64. Shabir, G.; Saeed, A.; Qasim, M.; Bolte, M.; Hökelek, T.; Erben, M. On the planarity of the cyclobutane ring in the crystal of dimethyl 2, 4-bis (3, 4-dimethoxyphenyl) cyclobutane-1, 3-dicarboxylate: a natural bond orbital and Hirshfeld surface analysis study. *New Journal of Chemistry* **2020**, *44*, 15515-15525, https://doi.org/10.1039/D0NJ02739A.
65. Shiroudi, A.; Safaei, Z.; Kazeminejad, Z.; Repo, E.; Pourshamsian, K. DFT study on tautomerism and natural bond orbital analysis of 4-substituted 1, 2, 4-triazole and its derivatives: solvation and substituent effects. *Journal of Molecular Modeling* **2020**, *26*, 1-11, https://doi.org/10.1007/s00894-020-4316-9.
66. Kia, R.; Kalaghchi, A. Structural, Non-Covalent Interaction, and Natural Bond Orbital Studies on Bromido-Tricarbonyl Rhenium (I) Complexes Bearing Alkyl-Substituted 1, 4-Diazabutadiene (DAB) Ligands. *Crystals* **2020**, *10*, https://doi.org/10.3390/cryst10040267.

67. Suvitha, A.; El-Mansy, M.; Kothandan, G.; Steephen, A. Molecular Structure, Ft-Raman, Ir, Nlo, Nbo, Homo–Lumo Analysis, Physicochemical Descriptors, Adme Parameters, And Pharmacokinetic Bioactivity Of 2, 3, 5, 6-Tetrachloro-p-Benzoquinone. *Journal of Structural Chemistry* **2021**, *62*, 1339-1356, https://doi.org/10.1134/S0022476621090031.
68. Akhtari, K.; Hassanzadeh, K.; Fakhraei, B.; Hassanzadeh, H.; Akhtari, G.; Zarei, S.A. First hyperpolarizability orientation in [70] PCBM isomers: A DFT study. *Computational and Theoretical Chemistry* **2014**, *1038*, 1-5, https://doi.org/10.1016/j.comptc.2014.03.036.
69. Abdelshafi, N.; Ibrahim, M.A.; Badran, A.-S.; Halim, S.A. Experimental and theoretical evaluation of a newly synthesized quinoline derivative as corrosion inhibitor for iron in 1.0 M hydrochloric acid solution. *Journal of Molecular Structure* **2021**, *1250*, https://doi.org/10.1016/j.molstruc.2021.131750.